Inorganic Chemistry Communications 185 (2026) 116058

Contents lists available at ScienceDirect

Inorganic Chemistry Communications

journal homepage: www.elsevier.com/locate/inoche

Short communication

Supramolecular coordination polymers, obtained from multidentate *N*′-benzoylpyrazine-2-carbohydrazonamide and a variety of salts PbX_2 (X = Cl^-, NO_3^-, NO_2^-, SCN^-), derived from tetrel and other noncovalent bonds

Ghodrat Mahmoudi [a,b], Isabel Garcia-Santos [c,*], Alfonso Castiñeiras [d], Atash V. Gurbanov [e], Ömer Faruk Tutar [f,g], Elizaveta V. Panova [h], Rosa M. Gomila [i], Antonio Frontera [i,*], Damir A. Safin [h,j,**]

[a] Department of Chemistry, Faculty of Science, University of Maragheh, P.O. Box 55136-83111, Maragheh, Iran
[b] Chemistry Department, Faculty of Engineering and Natural Sciences, Istinye University, Sariyer, Istanbul 34396, Turkey
[c] Departamento de Química Inorgánica, Facultad de Farmacia, Universidad de Santiago de Compostela, E-15782 Santiago de Compostela, Spain
[d] Department of Chemical and Pharmaceutical Sciences, University of Trieste, Via L. Giorgieri 1, 34127 Trieste, Italy
[e] Excellence Center, Baku State University, Z. Xalilov Str. 23, AZ 1148 Baku, Azerbaijan
[f] Department of Pharmacy Services, Vocational School of Health Care Services, Istinye University, Istanbul 34010, Turkey
[g] İstinye University, Scientific and Technological Research Application and Research Center, 34010 İstanbul, Turkey
[h] University of Tyumen, Volodarskogo Str. 6, 625003 Tyumen, Russian Federation
[i] Departament de Química, Universitat de les Illes Balears, crta. De Valldemossa km 7.5, 07122 Palma de Mallorca (Baleares), Spain
[j] Department of Chemistry, Dogus University, Dudullu-Ümraniye, 34775 Istanbul, Türkiye

ARTICLE INFO

Keywords:
Lead(II)
Hydrazone
Coordination polymer
Synthesis
Crystal structure
X-ray
DFT

ABSTRACT

Four lead(II) complexes, $[Pb(HL)Cl_2]$ (**1**), $[Pb(HL)_2(NO_3)_2]$ (**2**), $[PbL(NO_2)]$ (**3**) and $[PbL(NCS)(H_2O)]\cdot H_2O$ (**4**·H_2O), were synthesized from PbX_2 salts and the ligand *N*′-benzoylpyrazine-2-carbohydrazonamide (**HL**). Spectroscopic characterization confirmed that complexes **1** and **2** contain the neutral ligand (**HL**), while **3** and **4**·H_2O feature its deprotonated form (**L**). In all structures, the Pb^{2+} center is *N*,*N*′,*O*-chelated by the ligand. Bond length analysis revealed the longest Pb–N/O bonds in **2** due to coordination of two neutral HL ligands, whereas the deprotonated L^- in **3** and **4**·H_2O resulted in shorter Pb–N_{imine} and Pb–$O_{carbonyl}$ bonds. Secondary Pb···X tetrel bonds (X = Cl, N, O, S) form in complexes **1**, **3**, and **4**·H_2O due to coordination sphere gaps, leading to supramolecular 1D chains (**1**, **4**·H_2O) or a 2D sheet (**3**). These assemblies are further stabilized by extensive hydrogen bonding and π···π stacking interactions. The nature of the tetrel bonds was investigated using MEP surface analysis, dimerization energy calculations, and quantum chemical tools (QTAIM, NCIplot). Electron localization function (ELF) and Laplacian maps differentiated tetrel bonds from primary coordination bonds, and the energy contributions of coexisting tetrel and hydrogen bonds were quantified.

1. Introduction

The coordination chemistry of the lead(II) cation (Pb^{2+}) attracts considerable research interest due to its unique combination of properties. Its exceptionally large ionic radius and remarkably flexible range of attainable coordination numbers (often from 4 to 10) provide diverse structural possibilities. Critically, the stereochemically active $6s^2$ lone electron pair inherent to Pb^{2+} frequently induces significant distortions within its coordination sphere, leading to non-ideal geometries and asymmetric ligand environments [1–6]. Furthermore, tetrel bonding interactions, which are noncovalent forces arising from the electrophilic region on the Pb atom, are increasingly recognized as pivotal drivers in the self-assembly processes of the Pb^{2+}-based coordination polymers, significantly influencing their final architecture [7–12]. Consequently, the structural diversity observed in the Pb^2-derived coordination compounds arises from a complex interplay of factors: the nature of the organic ligands, the identity and influence of counterions, and the synergistic emergence of various supramolecular interactions, including

* Corresponding authors.
** Corresponding author at: University of Tyumen, Volodarskogo Str. 6, 625003 Tyumen, Russian Federation.
E-mail addresses: isabel.garcia@usc.es (I. Garcia-Santos), toni.frontera@uib.es (A. Frontera), damir.a.safin@gmail.com (D.A. Safin).

https://doi.org/10.1016/j.inoche.2025.116058
Received 27 September 2025; Received in revised form 24 November 2025; Accepted 17 December 2025
Available online 21 December 2025

tetrel bonding, hydrogen bonding, π···π stacking, etc., alongside the primary coordination bonds [10,13–16]. Notably, chelating ligands derived from hydrazones, containing N-donor rings, represent a versatile class, capable of binding metal centers like Pb^{2+} through their nitrogen atoms alongside other donor sites.

The concept of coordination polymers, extended structures formed by the linkage of metal centers via bridging ligands, has evolved significantly since its inception nearly nine decades ago with cyanide-based inorganic materials [17]. A pivotal shift occurred roughly 65 years ago with the first report of a coordination polymer constructed using an organic bridging ligand [18], paving the way for immense structural and functional diversity. The field has experienced accelerated growth over the last three decades, marked prominently by the emergence and explosive development of metal-organic frameworks (MOFs), a highly porous subclass of coordination polymers first described around 30 years ago [19,20]. Fundamentally, coordination polymers are characterized by their repeating coordination motifs, where metal cations or polynuclear clusters (nodes) are interconnected by multidentate organic ligands (linkers) to form extended architectures. These can manifest as one-dimensional (1D) chains, two-dimensional (2D) layers or networks, or three-dimensional (3D) frameworks [21], each with distinct properties and potential applications.

Designing effective ligands is paramount in the targeted synthesis of coordination polymers. Poly-N-donor molecules, ligands featuring multiple nitrogen donor atoms, remain one of the most prevalent and successful strategies for constructing robust coordination polymers [22]. Additionally, the Schiff base motif, characterized by an imine (azomethine) group –C=N–, serves as an exceptionally versatile and adaptable structural unit for the coordination polymer formation, offering synthetic tunability, diverse coordination possibilities, and potential sites for supramolecular interactions [23]. Recognizing the strengths of both approaches, the strategic integration of a Schiff base fragment with N-donor heterocyclic rings within a single ligand molecule presents a powerful dual-functionality approach. This combination leverages the chelating/stabilizing ability of the Schiff base and the directional bridging potential of the N-donor sites, offering enhanced control over network topology. Achieving such controlled assembly necessitates the use of reliable and well-understood synthetic "tools" – methodologies and ligand systems that are operationally accessible yet capable of yielding the desired and predictable architectures.

Beyond primary coordination bonds, exploiting noncovalent interactions is a highly effective strategy for directing the formation of extended supramolecular architectures or stabilizing specific coordination polymer conformations. In this context, tetrel bonding, particularly involving the electrophilic Pb center as the tetrel bond donor, has emerged as a potent and designable supramolecular synthon for constructing and stabilizing intricate structures. Our own studies have focused extensively on elucidating the coordination behavior of Pb^{2+}, with a specific emphasis on understanding and utilizing the synergy between conventional coordination bonds and tetrel bonding interactions for the deliberate construction of extended coordination polymers and intricate supramolecular assemblies [9–12,24–49].

In this work, we have strategically targeted the coordination chemistry arising from the interaction of a specifically prepared *N′*-benzoylpyrazine-2-carbohydrazonamide (**HL**) [50] with a variety of salts PbX_2 ($X = Cl^-$, NO_3^-, SCN^-) or a mixture of salts $Pb(NO_3)_2$ and $NaNO_2$. This ligand **HL**, featuring multiple potential donor sites, including pyrazine nitrogens, hydrazone functionalities, and carbonyl oxygen, was selected for its anticipated capacity to act as a versatile polydentate chelator and bridging unit, capable of engaging the Pb^{2+} ions in complex coordination modes. Following the synthesis under the applied conditions, the novel coordination compounds isolated from these reactions were subjected to comprehensive structural characterization. Initial insights into their chemical composition and bonding were obtained through FTIR spectroscopy, which probed key functional groups and coordination-induced shifts. Solution-state behavior and ligand environment were further elucidated by ^{1}H NMR spectroscopy in DMSO-d_6. Critically, the crystal structures of the isolated complexes were elucidated using single-crystal X-ray diffraction, providing unambiguous evidence of the molecular architecture, metal coordination sphere geometry and overall supramolecular organization within the crystalline solids. This work also provides a comprehensive theoretical analysis of the Pb···X tetrel bonds present in the solid-state structures of complexes **1**, **3** and **4**. We employed density functional theory (DFT) to compute dimerization energies and characterize the nature of these interactions using molecular electrostatic potential (MEP) surfaces, quantum theory of atoms in molecules (QTAIM), and Non-Covalent Interaction (NCIplot) index analyses. The contribution of the tetrel bonds was also compared to that of the coordination bonds using 2D maps of the electron localization function (ELF) and the Laplacian of the electron density. For systems where hydrogen bonds co-exist with tetrel bonds, we estimated the relative energetic contribution of each by calculating the potential energy density at the respective bond critical points.

2. Experimental

2.1. Materials and physical measurements

All reagents and solvents were commercially available and used without further purification. The FTIR spectra were obtained with a BRUKER IFS-66v spectrometer. The ^{1}H NMR spectra in DMSO-d_6 were recorded with a Bruker DPX FT/NMR-400 spectrometer. Microanalyses were performed using a LECO-elemental analyzer.

2.2. Synthesis

A solution of PbX_2, where $X = Cl^-$, NO_3^- or SCN^- (22.2, 26.5 and 25.9 mg, respectively; 0.08 mmol) or a mixture of $Pb(NO_3)_2$ (26.5 g, 0.08 mmol) and $NaNO_2$ (11.0 mg, 0.16 mmol) in distilled water (2 mL) was added to a solution of **HL** (19.3 mg, 0.08 mmol) in methanol (25 mL). The resulting mixture was stirred for 1 h and left undisturbed for slow evaporation under ambient conditions, yielding crystals suitable for single-crystal X-ray analysis after several days.

[Pb(HL)Cl_2] (1). Orange needle-like crystals. Yield: 12.5 mg (30 %). ^{1}H NMR, *δ*: 7.06 (br. s, 2H, NH_2), 7.50 (t, $^3J_{H,H} = 7.3$ Hz, 2H, *m*-H, Ph), 7.56 (t, $^3J_{H,H} = 7.3$ Hz, 1H, *p*-H, Ph), 7.89 (d, $^3J_{H,H} = 7.4$ Hz, 2H, *o*-H, Ph), 8.68 (br. s, 1H, 6-H, pyrazine), 8.73 (br. s, 1H, 5-H, pyrazine), 9.34 (br. s, 1H, 3-H, pyrazine), 10.33 (s, 1H) ppm. Anal. calc. for $C_{12}H_{11}Cl_2N_5OPb$ (519.36): C 27.75, H 2.13 and N 13.48 %; found: C 27.88, H 2.08 and N 13.57 %.

[Pb(HL)$_2$(NO_3)$_2$] (2). Yellow block-like crystals. Yield: 14.3 mg (44 %). ^{1}H NMR, *δ*: 7.25–7.76 (m, 5H, *m*-H + *p*-H + NH_2, Ph + NH_2), 7.93 (br. s, 2H, *o*-H, Ph), 8.75 (br. s, 1H, 6-H, pyrazine), 8.81 (br. s, 1H, 5-H, pyrazine), 9.37 (br. s, 1H, 3-H, pyrazine), 10.55 (s, 1H) ppm. Anal. calc. for $C_{24}H_{22}N_{12}O_8Pb$ (813.71): C 35.43, H 2.73 and N 20.66 %; found: C 35.36, H 2.69 and N 20.74 %.

[PbL(NO_2)] (3). Orange pat-like crystals. Yield: 13.8 mg (35 %). ^{1}H NMR, *δ*: 7.33–7.48 (m, 3H, *m*-H + *p*-H, Ph), 7.70 (br. s, 2H, NH_2), 8.19–8.33 (m, 2H, *o*-H, Ph), 8.90 (br. s, 1H, 6-H, pyrazine), 8.98 (d, $^4J_{H,H} = 2.5$ Hz, 1H, 5-H, pyrazine), 9.48 (d, $^4J_{H,H} = 1.5$ Hz, 1H, 3-H, pyrazine) ppm. Anal. calc. for $C_{12}H_{10}N_6O_3Pb$ (493.45): C 29.21, H 2.04 and N 17.03 %; found: C 29.30, H 2.09 and N 16.95 %.

[PbL(SCN)H_2O]·H_2O (4·H_2O). Yellow needle-like crystals. Yield: 23.4 mg (54 %). ^{1}H NMR, *δ*: 7.38–7.46 (m, 3H, *m*-H + *p*-H, Ph), 7.80 (br. s, 2H, NH_2), 8.26–8.32 (m, 2H, *o*-H, Ph), 8.92–8.98 (m, 1H, 6-H, pyrazine), 9.01 (d, $^4J_{H,H} = 2.4$ Hz, 1H, 5-H, pyrazine), 9.51 (d, $^4J_{H,H} = 1.5$ Hz, 1H, 3-H, pyrazine) ppm. Anal. calc. for $C_{13}H_{14}N_6O_3PbS$ (541.55): C 28.83, H 2.61 and N 15.52 %; found: C 28.72, H 2.65 and N 15.47 %.

2.3. Crystal structure

The X-ray diffraction data were collected at 100(2) K on a Bruker APEX-II CCD diffractometer (Mo-Kα, λ = 0.71073 Å, graphite monochromator). The data were processed with APEX2 [51] and corrected for absorption using SADABS [52]. The structure was solved by direct methods using the program SHELXS-97 [53] and refined by the full-matrix least-squares technique using SHELXL-2013 [53]. All non-hydrogen atoms were refined with anisotropic displacement parameters and the hydrogen atoms were placed at calculated positions. CCDC 2483437–2483440 contain the supplementary crystallographic data. These data can be obtained free of charge via https://www.ccdc.cam.ac.uk/structures or from the Cambridge Crystallographic Data Centre, 12 Union Road, Cambridge CB2 1EZ, UK; fax: (+44)-1223–336-033; or e-mail: deposit@ccdc.cam.ac.uk.

Crystal data for 1. $C_{12}H_{11}Cl_2N_5OPb$, M_r = 519.35, triclinic, space group $P\bar{1}$, a = 7.8814(10) Å, b = 9.0983(11) Å, c = 11.0235(14) Å, α = 67.180(5)°, β = 89.534(5)°, γ = 88.812(5)°, V = 728.44(16) Å^3, Z = 2, ρ = 2.368 g cm^{-3}, μ(Mo-Kα) = 11.952 mm^{-1}, reflections: 72368 collected, 8216 unique, R_{int} = 0.056, R_1(all) = 0.0169, wR_2(all) = 0.0352, S = 1.045.

Crystal data for 2. $C_{24}H_{22}N_{12}O_8Pb$, M_r = 813.72, monoclinic, space group $C2/c$, a = 13.4000(8), b = 14.653(1), c = 15.5343(10) Å, β = 112.619(2)°, V = 2815.6(3) Å^3, Z = 4, ρ = 1.920 g cm^{-3}, μ(Mo-Kα) = 6.064 mm^{-1}, reflections: 101259 collected, 4294 unique, R_{int} = 0.054, R_1(all) = 0.0131, wR_2(all) = 0.0304, S = 1.082.

Crystal data for 3. $C_{12}H_{10}N_6O_3Pb$, M_r = 493.45, monoclinic, space group $P2_1/n$, a = 9.0062(4), b = 16.0716(8), c = 9.6479(5) Å, V = 1362.65(12) Å^3, Z = 4, ρ = 2.405 g cm^{-3}, μ(Mo-Kα) = 12.405 mm^{-1}, reflections: 87313 collected, 4159 unique, R_{int} = 0.069, R_1(all) = 0.0362, wR_2(all) = 0.0657, S = 1.060.

Crystal data for 4·H$_2$O. $C_{13}H_{15}N_6O_3PbS_2$, M_r = 541.55, triclinic, space group $P\bar{1}$, a = 7.1636(3) Å, b = 10.6628(4) Å, c = 11.3512(4) Å, α = 104.567(2)°, β = 91.260(2)°, γ = 107.331(1)°, V = 796.66(5) Å^3, Z = 2, ρ = 2.258 g cm^{-3}, μ(Mo-Kα) = 10.746 mm^{-1}, reflections: 98669 collected, 9013 unique, R_{int} = 0.069, R_1(all) = 0.0224, wR_2(all) = 0.0394, S = 1.043.

2.4. Theoretical methods

The geometries of the complexes were optimized based on their crystallographic coordinates using the PBE0-D4/def2-TZVP level of theory [54–56]. All calculations were carried out with the TURBOMOLE 7.7 software package [57]. Electron density analysis was performed using the "atoms-in-molecules" (AIM) method [58]. This analysis, along with the computation of electron density vs. electrostatic potential plots, 2D reduced density gradient (RDG) [59] and 2D electron localization function (ELF) [60] plots, was conducted using the Multiwfn program [61]. The visualization of the QTAIM analysis was generated with VMD software [62]. To further characterize the interactions, the Laplacian of the electron density ($\nabla^2\rho$) was decomposed into its three principal eigenvalues (λ_1, λ_2, λ_3). The sign of the second eigenvalue, λ_2, is used to distinguish between different types of interactions. Specifically, a negative λ_2 value ($\lambda_2 < 0$) indicates an attractive bonding interaction, while a positive value ($\lambda_2 > 0$) signifies a non-bonding or repulsive interaction.

3. Results and discussion

An aqueous solution of PbX_2 (X = Cl^-, NO_3^-, SCN^-) or a mixture of salts $Pb(NO_3)_2$ and $NaNO_2$ was reacted with a methanolic solution of **HL**, yielding orange or yellow crystals of new coordination compounds [Pb(HL)Cl$_2$] (**1**), [Pb(HL)$_2$(NO$_3$)$_2$] (**2**), [PbL(NO$_2$)] and [PbL(NCS)(H$_2$O)]·H$_2$O (**4**·H$_2$O) after standing undisturbed under ambient conditions (Scheme 1). Notably, the isolated crystals of all the complexes were suitable for a single crystal X-ray diffraction analysis; thus, no recrystallization was required. The formation of the resulting complexes was supported by the elemental analysis data and their structures were further characterized by the means of the FTIR and ^{1}H NMR spectroscopy. The crystal structures were revealed by single crystal X-ray diffraction. Interestingly, the parent organic ligand is involved in its neutral form in complexes **1** and **2**, while complexes **3** and **4**·H$_2$O contain the deprotonated form **L** (Scheme 1). Thus, we can tentatively

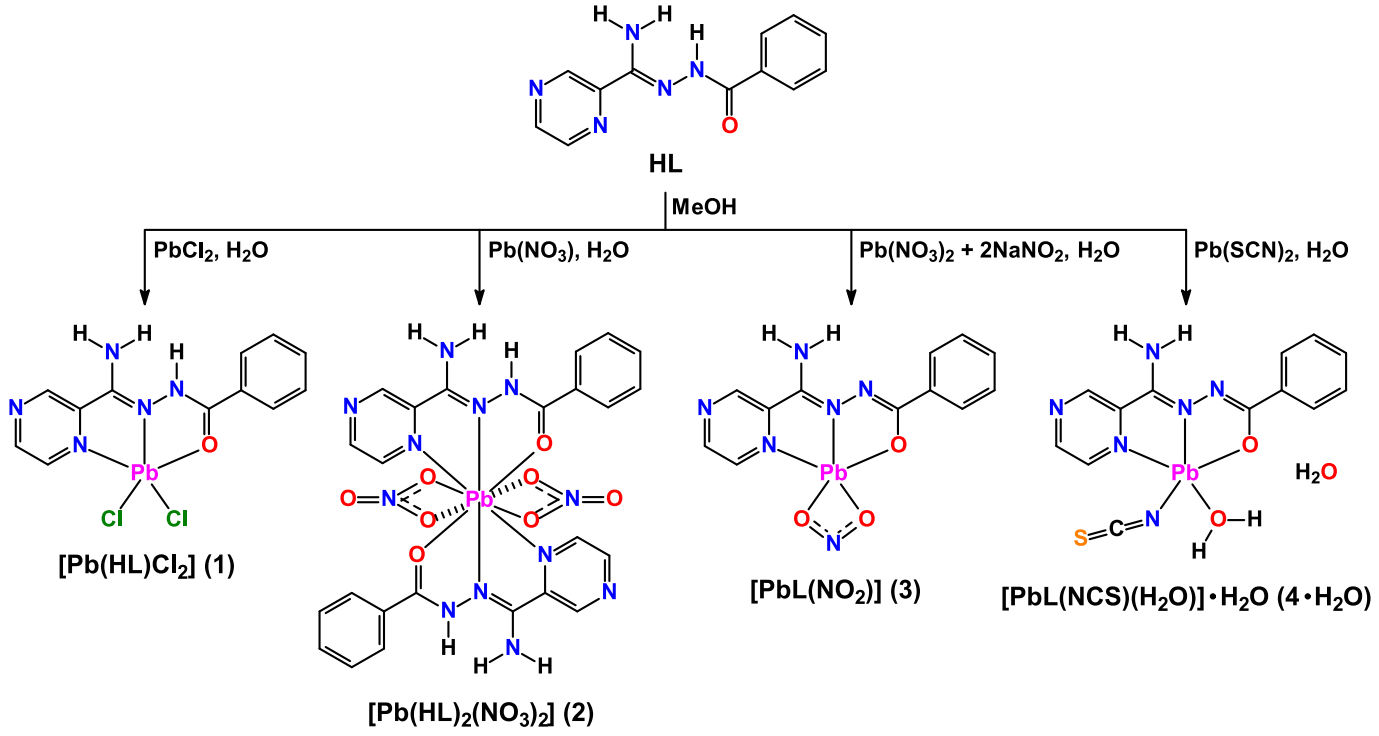

Scheme 1. Synthesis of the title complexes.

conclude that the presence of the Pb^{2+}–NO_2^- and Pb^{2+}–NCS^- systems induce the deprotonation of **HL** under the applied synthetic conditions.

The FTIR spectra of the obtained complexes each contain a set of bands from about 2900 cm^{-1} to 3550 cm^{-1}, which correspond to CH and NH_2 vibrations (Fig. 1). This range of the IR spectra of complexes **1** and **2** are further complicated by the presence of bands for the amide NH group, while in the spectrum of complex **4**·H_2O the bands for both the coordinated and crystal water molecules also contribute to the same range (Fig. 1). The NH_2 group is also shown in the spectra of the title complexes with the bands at about 670–710 cm^{-1} due to out-of-plane N–H bending (Fig. 1). The spectra of complexes **2** and **3** exhibit an intense band at 1290 and 1360 cm^{-1}, corresponding to the NO_3^- and NO_2^- anions, respectively (Fig. 1). The spectrum of complex **4**·H_2O exhibits an intense band at 2040 cm^{-1}, which is characteristic for the isothiocyanate CN group (Fig. 1). Furthermore, the libration and bending bands of the water molecules are shown in the spectrum of complex **4**·H_2O as two broad profiles at about 500–700 and 1550–1650 cm^{-1}, respectively (Fig. 1). Finally, the band for the carbonyl group is found in the spectra of complexes **1** and **2** at about 1670–1675 cm^{-1}, while the same band in the spectra of complexes **3** and **4**·H_2O was found at about 1620 cm^{-1} (Fig. 1). This band in the spectra of the former two complexes is about 30–35 cm^{-1} shifted to higher wavenumbers, while in the spectra of the latter two complexes is about 20–25 cm^{-1} shifted to lower wavenumbers in comparison to that in the spectrum of the parent ligand **HL** [50]. This, obviously, is explained by the neutral and deprotonated forms of the organic ligand in the structures of complexes **1** and **2**, and **3** and **4**·H_2O, respectively.

The ^{1}H NMR spectrum of complex **1** in DMSO-d_6 (Fig. 2) is very similar to that of the parent ligand **HL**, recorded in the same solvent [50]. In particular, the spectrum of complex **1** contains two triplets at 7.50 and 7.56 ppm, and one doublet at 7.89 ppm, corresponding to the *m*-, *p*- and *o*-H atoms of the phenyl group, while the pyrazine hydrogens were shown as three broad singlets at 8.68, 7.73 and 9.34 ppm, corresponding to the 6-, 5- and 3-H atoms (Fig. 2). The NH_2 and NH hydrogens were found in the spectrum of complex **1** as broad and narrow singlets at 7.06 and 10.33 ppm, respectively (Fig. 2). The ^{1}H NMR spectrum of complex **2** recorded in the same solvent is similar to that of complex **1**; however, all the signals are significantly broadened (Fig. 2).

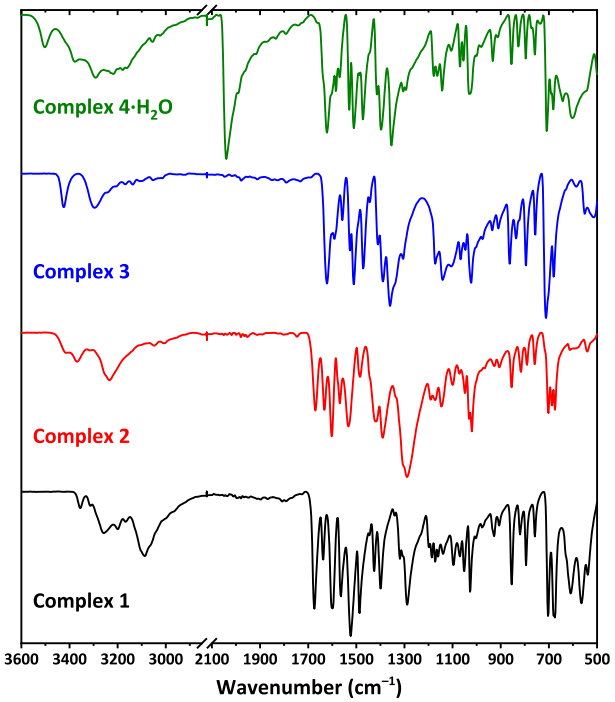

Fig. 1. The FTIR spectra of the title complexes.

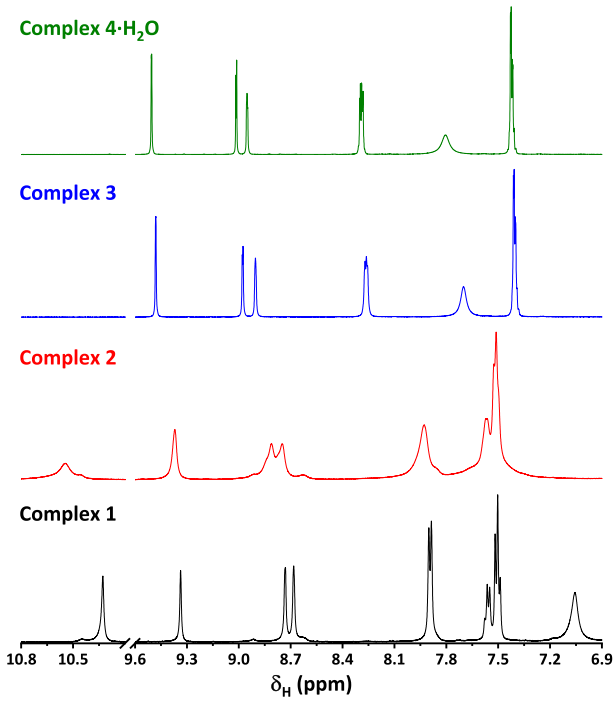

Fig. 2. The ^{1}H NMR spectra of the title complexes recorded in DMSO-d_6.

Furthermore, the signals for the phenyl *m*- and *p*-H atoms are significantly overlapped with the signal for the NH_2 hydrogens (Fig. 2). The ^{1}H NMR spectra of complexes **3** and **4**·H_2O obtained in DMSO-d_6 are very similar but exhibit clear differences. In particular, the *m*- and *p*-H atoms were found in the spectra as a multiplet at 7.33–7.48 ppm, while the *o*-H atoms were shown as a multiplet at 8.19–8.33 ppm (Fig. 2). The pyrazine hydrogens were observed in the spectra as a broad singlet or a miltiplet at 8.90–8.98 ppm, and as two doublets at 8.98–9.01 and 9.48–9.51 ppm (Fig. 2). The NH_2 hydrogens were revealed in the spectra as a broad singlet at 7.70–7.80 ppm (Fig. 2). Notably, no signal for the amide NH hydrogen atom was found in the spectra of complexes **3** and **4**·H_2O, thus, testifying to the deprotonated form of the organic ligand in their structures.

Thus, comparison of the FTIR and ^{1}H NMR spectra of the discussed complexes with those of the parent ligand **HL** [50] supports the formation of complex **1–4**·H_2O.

The crystal structures of complexes **1** and **4**·H_2O were solved in triclinic space group $P\bar{1}$, while the structures of complexes **2** and **3** were solved in monoclinic space groups $C2/c$ and $P2_1/n$, respectively. The asymmetric units of **1–3** contain one Pb^{2+} cation, one ligand **HL** (in **1** and **2**) or **L** (in **3**), and two chlorine or one nitrate or one nitrite anions. The asymmetric unit of **4**·H_2O contains one Pb^{2+} cation, one ligand **L**, one isothiocyanate anion, one coordinated and one crystal water molecules. The Pb^{2+} cation in the structures of all complexes is *N*,*N*′,*O*-chelated either by the ligand **HL** or **L** through the pyrazine and imine nitrogen atoms, and the carbonyl oxygen atom (Fig. 3). The Pb–$N_{pyrazine}$, Pb–N_{imine} and Pb–$O_{carbonyl}$ bonds are about 2.64, 2.51 and 2.46 Å in the crystal structure of complex **1**. The former bond is about 0.05–0.06 Å longer, while the latter two bonds are about 0.10–0.13 and 0.06–0.15 Å shorter in the crystal structures of complexes **3** and **4**·H_2O (Table 1). Notably, the same bonds in the crystal structure of **2** are the longest within the whole series of the studied complexes, and of about 2.85, 2.64 and 2.55 Å, respectively (Table 1). All these trends are explained by the neutral and deprotonated forms of the organic ligands in the structures of **1** and **2**, and **3** and **4**·H_2O, respectively. Furthermore, the longest Pb–N and Pb–O coordination bonds in the structure of complex **2** is due to coordination of two organic ligands **HL**, while the other three complexes comprise only one ligand **HL** or one ligand **L**.

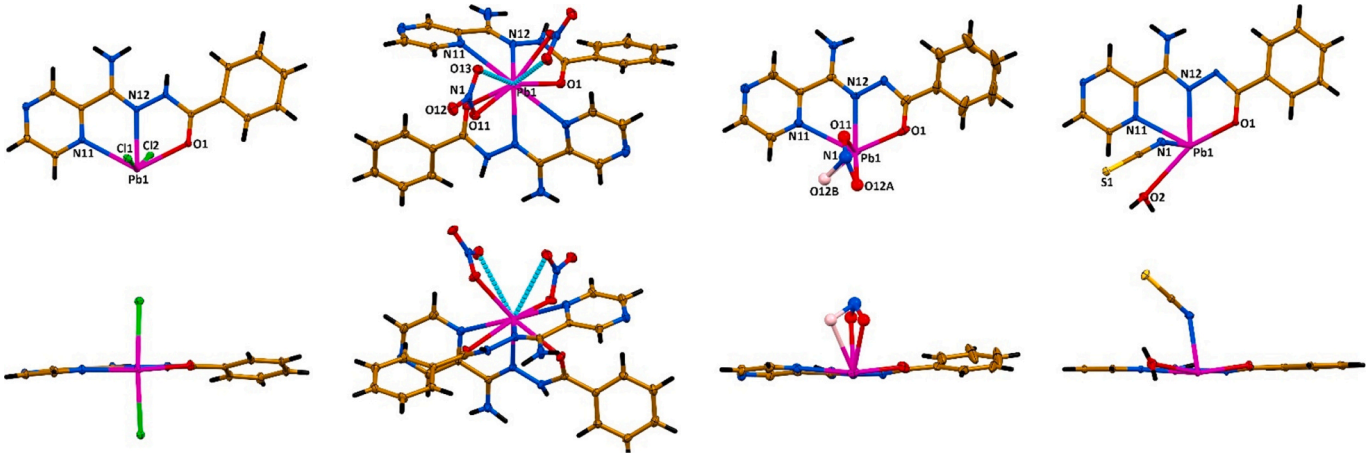

Fig. 3. Top (top) and side (bottom) views of the molecular structures of complexes **1–4** (from left to right). The minor occupancy of one of the NO_2^- oxygen atoms is shown in pink. Colour code: H = black, C = gold, N = blue, O = red, Cl = green, S = yellow, Pb = magenta. (For interpretation of the references to colour in this figure legend, the reader is referred to the web version of this article.)

Table 1
Selected bond lengths (Å) in the crystal structures of the title complexes.[a]

Bond	Length	Type	Bond	Length	Type
*Complex **1***					
Pb1–N11	2.6415(12)	Covalent	Pb1–Cl2	3.2705 (6)	Covalent
Pb1–N12	2.5070(13)	Covalent	Pb1···Cl1$^{\#1}$	3.4178(6)	Tetrel
Pb1–O1	2.4632(11)	Covalent	Pb1···Cl2$^{\#2}$	3.2705 (6)	Tetrel
Pb1–Cl1	2.9162(5)	Covalent			
*Complex **2***					
Pb1–N11	2.8465(15)	Covalent	Pb1–O11	2.7399(10)	Covalent
Pb1–N12	2.6376(13)	Covalent	Pb1···O13$^{\#3}$	3.2051 (12)	Tetrel
Pb1–O1	2.5533(12)	Covalent			
*Complex **3***					
Pb1–N11	2.699(4)	Covalent	Pb1–O12B	2.702(8)	Covalent
Pb1–N12	2.377(4)	Covalent	Pb1···N13$^{\#4}$	3.234(4)	Tetrel
Pb1–O1	2.312(3)	Covalent	Pb1···N15$^{\#5}$	3.657(5)	Tetrel
Pb1–O11	2.432(4)	Covalent	Pb1···O12A$^{\#6}$	2.955(8)	Tetrel
Pb1–O12A	2.676(8)	Covalent			
*Complex **4**·H_2O*					
Pb1–N11	2.6852(13)	Covalent	Pb1–O2	2.8986(13)	Covalent
Pb1–N12	2.4056(14)	Covalent	Pb1···N13$^{\#1}$	3.0466(14)	Tetrel
Pb1–N1	2.4358(15)	Covalent	Pb1···N16$^{\#1}$	3.5248(15)	Tetrel
Pb1–O1	2.3979(11)	Covalent	Pb1···S1$^{\#7}$	3.3377(5)	Tetrel

[a] Symmetry codes: #1 2 – *x*, 2 – *y*, –*z*; #2 1 – *x*, 2 – *y*, –*z*; #3 1 – *x*, *y*, 1/2 – *z*; #4 *x*, *y*, 1 + *z*; #5 1/2 – *x*, –1/2 + *y*, 1/2 – *z*; #6 1 – *x*, 1 – *y*, 1 – *z*; #7 1 – *x*, 1 – *y*, –*z*.

The Pb–Cl bond lengths in the structure of complex **1** differ significantly. While one bone is about 2.92 Å, the second bond is about 0.35 Å longer (Table 1). It should be noted that one of the nitrite oxygen atoms in the structure of complex **3** is disordered over two positions with a ratio of 51.8 % to 48.2 %. The Pb–O bond lengths formed with the nitrite oxygen atoms are about 2.43 and 2.68–2.70 Å, indicating the chelating nitrito nature. The nitrate anions in the structure of complex **2** are coordinated in an anisobidentate manner as evidenced from the criteria reported previously [63], yielding two additional Pb–O tetrel bonds. Particularly, the Δd values are about 0.47 Å and the $\Delta\theta$ values are about 22°. In the structure of complex **4**·H_2O, the Pb–NCS bond length is similar to those formed with the imine nitrogen and carbonyl oxygen atoms, and of about 2.44 Å, while the Pb–O bond length formed with the coordinated water molecule is the longest among the coordination bonds and of about 2.90 Å (Table 1). The monodentate N-coordination mode of the isothiocyanate anion revealed the Pb–N–C and N=C=S bond angles of about 131 and 179°, indicating a linear structure of this anion (Fig. 3). Interestingly, the angles formed by the mean planes of the pyrazine and phenyl rings are about 17.8, 3.2, 21.4 and 2.3° in the structures of complexes **1–4**·H_2O, respectively. This indicate an almost planar structure of the ligand **L** in complex **4**·H_2O, while the ligands **HL** and **L** are somewhat deviated from planarity in the structures of complexes **1** and **3**, mainly due to a rotation of the phenyl ring (Fig. 3). However, while the angle between the mean planes formed by the pyrazine and phenyl rings is also impoverished in complex **2**, the ligand **HL** is markedly deviated from planarity due to a distorted chelate backbone (Fig. 3).

The covalent bonds in the structures of complexes **1**, **3** and **4**·H_2O are collected on an almost quarter (in **3**) or on an almost half (in **1** and **4**·H_2O) of the globe of the coordination sphere yielding a large gap in the coordination spheres of the metal cations (Fig. 3). This gap enables a close approach of the two chlorine atoms from two adjacent molecules in the structure of complex **1**, yielding two Pb···Cl tetrel bonds; one amide and one pyrazine nitrogen atoms, and one of the nitrite oxygen atoms from three neighboring molecules in the structure of complex **3**, yielding two Pb···N and one Pb···O tetrel bonds; one amide and one amine nitrogen atoms from an adjacent molecule, and one isothiocyanate sulfur atom from the second molecule in the structure of complex **4**·H_2O, yielding two Pb···N and one Pb···S tetrel bonds. Considering all the covalent and tetrel bonds, the coordination sphere in the structures of complexes **1–4**·H_2O is described as seven N_2OCl_4, ten N_4O_6, eight N_4O_4 and eight N_5O_2S environments, respectively. According to the

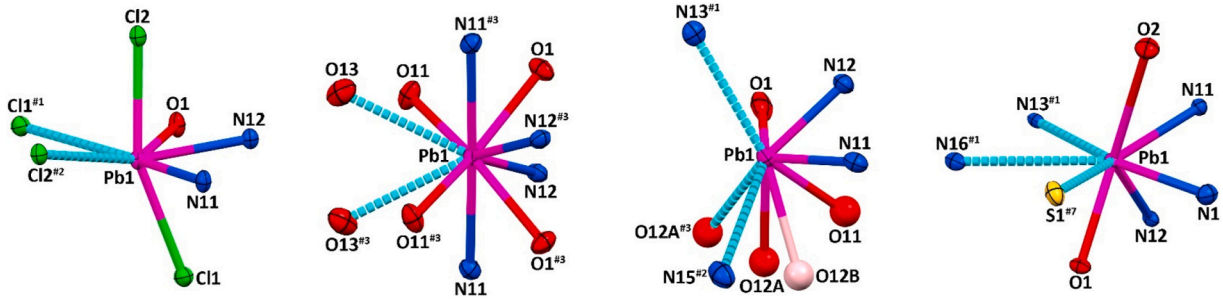

Fig. 4. Coordination environments in the structures of complexes **1–4** (from left to right), constructed through the Pb–N, Pb–O and Pb–Cl coordination bonds, and Pb···N, Pb···O, Pb···Cl and Pb···S tetrel bonds.

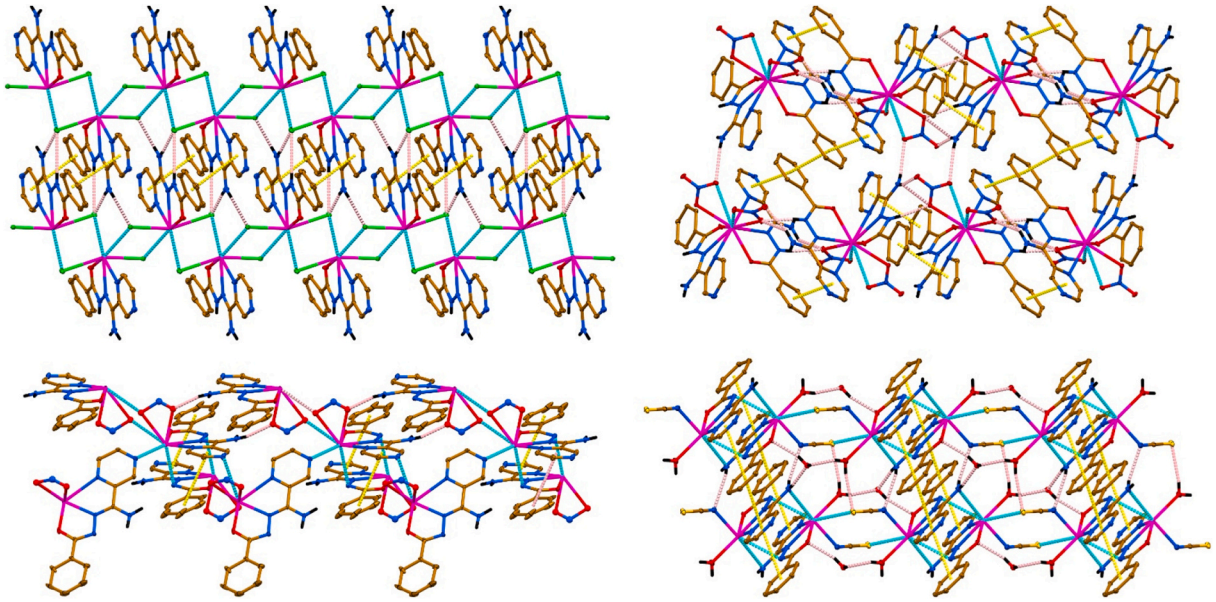

Fig. 5. Supramolecular aggregates in the structures of complexes **1** (top-left), **2** (top-right), **3** (bottom-left) and **4**·H_2O (bottom-right), constructed through the Pb···N, Pb···O, Pb···Cl and Pb···S tetrel bonds; N–H···N, N–H···O, N–H···Cl, O–H···N, O–H···O and O–H···S hydrogen bonds; and π···π interactions. CH hydrogen atoms were omitted for clarity. Colour code: H = black, C = gold, N = blue, O = red, Cl = green, S = yellow, Pb = magenta; Pb···N, Pb···O, Pb···Cl and Pb···S tetrel bonds = cyan dashed line; N–H···N, N–H···O, N–H···Cl, O–H···N, O–H···O and O–H···S hydrogen bonds = pink dashed line; π···π interactions = yellow dashed line. (For interpretation of the references to colour in this figure legend, the reader is referred to the web version of this article.)

SHAPE software terminology [64], these polyhedra were found to be close to the capped trigonal prism in complex **1**, metabidiminished icosahedron J62 in complex **2**, triangular dodecahedron or square antiprism in complex **3**, and triangular dodecahedron or square antiprism or Johnson gyrobifastigium J26 in complex **4**·H_2O (Fig. 4).

The formation of tetrel bonds leads to a 1D supramolecular chain in the structures of complexes **1** and **4**·H_2O, and a 2D supramolecular sheet in the structure of complex **3** (Fig. 5). Furthermore, all the reported complexes are characterized by te formation of extended structures due to a rich variety of hydrogen bonds formed with the participation of the NH_2 and NH hydrogens and chlorine atoms, or nitrate and nitrite oxygen atoms in complexes **1–3** (Fig. 5, Table 2). In complex **4**·H_2O, the hydrogen atoms of the NH_2, coordinated and crystal water molecules form hydrogen atoms with the carbonyl and crystal water oxygen atoms, and isothiocyanate nitrogen and sulfur atoms (Fig. 5, Table 2).

The supramolecular structures of the title complexes are reinforced by π···π interactions formed between the pyrazine and phenyl rings (Fig. 5, Table 3). The structures of complexes **1** and **2** are further stabilized by π···π interactions formed between the phenyl rings (Fig. 5, Table 3).

The crystal structures of complexes **1**, **3** and **4** reveal the crucial role of tetrel bonds in their supramolecular assembly. To provide a deeper understanding of these non-covalent interactions, we performed a detailed theoretical analysis based on the experimental geometries.

In complex **1**, the most negative MEP is located at the Cl anion (−52.0 kcal/mol), followed by the carbonyl oxygen atom (−21.9 kcal/mol) and the pyrazine free nitrogen atom (−15.7 kcal/mol) (Fig. 6). The positive regions are most pronounced at the hydrogen atoms, with the highest MEP values located at the NH_2 hydrogen atoms (84.7 and 69.0 kcal/mol) (Fig. 6). The MEP is also positive over the pyrazine ring (18.1 kcal/mol) and neutral (0.0 kcal/mol) over the phenyl ring (Fig. 6). The MEP surface around the Pb atom reveals two regions of positive potential at the molecular plane, with values of 31.2 and 15.6 kcal/mol (Fig. 6). The strongest of these is likely influenced by the proximity of the pyrazine C–H bond (Fig. 6). This MEP distribution aligns well with the supramolecular aggregate observed in the crystal structure of **1**.

For complex **3**, the minimum MEP is found at the nitrite oxygen atom (−54.0 kcal/mol), followed by the carbonyl oxygen atom (−39.5 kcal/mol) (Fig. 6). The anionic nature of the organic ligand in **3**, unlike that in **1**, results in a large negative potential over the phenyl ring (−17.6 kcal/mol), while the potential over the pyrazine ring is positive (32.2 kcal/mol) (Fig. 6), a condition that facilitates π···π interaction. The MEP at the free pyrazine nitrogen atom is negative (−15.7 kcal/mol). The MEP maxima are located at the NH_2 hydrogen atoms (59.6 and 36.4 kcal/

Table 2
Hydrogen bond lengths (Å) and angles (°) in the crystal structures of the title complexes.

D–H···A	*d*(D–H)	*d*(H···A)	*d*(D···A)	∠(DHA)	Symmetry code
*Complex **1***					
N13–H13A···Cl1	0.79	2.80	3.5808(14)	173	2 – *x*, 1 – *y*, −*z*
N16–H16A···Cl2	0.86	2.34	3.1705 (13)	163	*x*, −1 + *y*, *z*
N16–H16B···Cl1	0.87	2.29	3.1370 (13)	164	2 – *x*, 1 – *y*, −*z*
*Complex **2***					
N13–H13A···O11	0.84	2.04	2.8718(16)	172	1 – *x*, −*y*, −*z*
N16–H16A···O11	0.94	2.43	3.1153 (17)	130	1 – *x*, −*y*, −*z*
N16–H16A···O12	0.94	2.06	2.9638(18)	161	1 – *x*, −*y*, −*z*
N16–H16B···O13	0.78	2.28	2.935(2)	142	1/2 + *x*, 1/2 + *y*, *z*
*Complex **3***					
N16–H16A···O11	0.93	2.08	2.979(6)	162	–*x*, 1 – *y*, −*z*
*Complex **4**·H$_2$O*					
N16–H16A···N1	0.90	2.44	3.159(2)	138	*x*, 1 + *y*, *z*
N16–H16B···O3	0.83	2.03	2.8270(19)	160	*x*, 1 + *y*, −1 + *z*
O2–H2A···O3	0.82	2.06	2.8622(18)	167	*x*, *y*, −1 + *z*
O2–H2B···S1	0.86	2.55	3.3933(16)	167	2 – *x*, 1 – *y*, −*z*
O3–H3A···N15	0.84	1.99	2.8361(18)	176	1 – *x*, 1 – *y*, −*z*
O3–H3B···O1	0.82	2.02	2.8155(18)	163	1 – *x*, 1 – *y*, 1 – *z*

mol) (Fig. 6). The MEP at the Pb atom shows three regions of high positive potential or σ-holes: one perpendicular to the ligand molecular plane (22.6 kcal/mol) and two within the plane (27.6 and 18.2 kcal/mol) (Fig. 6). As with complex **1**, the largest σ-hole is influenced by the nearby pyrazine C–H bond.

In complex **4**, the MEP minimum is at the thiocyanate anion (−40.8 kcal/mol), followed by the carbonyl oxygen atom (−37.0 kcal/mol) and the pyrazine nitrogen atom (−20.7 kcal/mol) (Fig. 6). The phenyl ring also shows a negative potential (−18.8 kcal/mol), while the pyrazine ring is positive (20.7 kcal/mol) (Fig. 6), a pattern that facilitates π···π interaction. The MEP maxima is located at the hydrogen atoms of the coordinated water molecule (61.5 kcal/mol), followed by the NH_2 hydrogen atoms (56.5 and 35.1 kcal/mol). Similar to complex **3**, the Pb atom in **4** exhibits three preferential regions of positive potential: the most positive is perpendicular to the ligand plane (35.8 kcal/mol), with other positive regions at the molecular plane (30.1 and 25.7 kcal/mol) (Fig. 6).

Overall, the MEP analysis confirms the presence of strong hydrogen bond donor and acceptor sites within these complexes as well as electron-deficient and electron-rich aromatic rings that can participate in charge-assisted π···π interactions. Critically, the MEP around the Pb atom is found to be highly anisotropic, with distinct regions of positive potential (σ-holes), making it well-suited for engaging in tetrel bonding interactions.

Two self-assembled tetrel bonded dimers in the structure of complex **1** were examined using the QTAIM/NCIplot analysis. The dominant dimer in the solid state, with a total dimerization energy of −26.5 kcal/mol, is characterized by a prominent Pb···Cl tetrel bond, identified by a bond critical point and a corresponding bond path (Fig. 7). Additionally, the analysis reveals two ancillary C–H···Cl hydrogen bonds which also contribute to the dimer's formation (Fig. 7). Using the NCIplot analysis, all interactions were further characterized by green, disk-shaped reduced density gradient isosurfaces, which discloses their attractive nature (Fig. 7). The energetic contribution of these hydrogen bonds was estimated using the potential energy density (V(r)) at the bond critical point, following the relationship $E = 0.5$ V proposed by Espinosa et al. [65]. The hydrogen bonds contribute only −4.0 kcal/mol to the total energy, confirming that the tetrel bond is the dominant interaction in this dimer (Fig. 7). A second self-assembled tetrel-bonded dimer has a significantly smaller dimerization energy of −12.9 kcal/mol (Fig. 7). In this dimer, each Pb atom forms a bifurcated contact, interacting not only with a Cl atom but also with the carbonyl oxygen atom (Fig. 7). These interactions are confirmed by the presence of bond critical points and bond paths, which are also characteristic of bifurcated Pb···Cl/O contacts (Fig. 7). The lower dimerization energy of this dimer is in good agreement with the MEP analysis, which showed a significantly less positive σ-hole adjacent to the oxygen atom, indicating a weaker interaction compared to the Pb···Cl bond in the other dimer that used the σ-hole adjacent to the C–H bond.

The self-assembled dimer of complex **3** is held together by a single Pb···N tetrel bond as indicated by the presence of a bond critical point and a bond path connecting the Pb atom to a pyrazine nitrogen atom of a

Table 3
π···π interaction lengths (Å) and angles (°) in the crystal structures of the title complexes.

Cg(*I*)	Cg(*J*)	*d*[Cg(*I*)···Cg(*J*)]	*α*	*β*	*γ*	Slippage	Symmetry code
*Complex **1***							
Pyrazine	Phenyl	3.8233(10)	17.80(7)	28.5	10.7	1.822	2 – *x*, 1 – *y*, −*z*
Phenyl	Pyrazine	3.8233(10)	17.80(7)	10.7	28.5	0.708	2 – *x*, 1 – *y*, −*z*
Phenyl	Phenyl	3.6288(10)	0.00(7)	22.3	22.3	1.377	2 – *x*, 1 – *y*, 1 – *z*
*Complex **2***							
Pyrazine	Phenyl	3.9207(9)	3.16(7)	28.0	30.6	1.840	1 – *x*, −*y*, −*z*
Phenyl	Pyrazine	3.9207(9)	3.16(7)	30.6	28.0	1.996	1 – *x*, −*y*, −*z*
Phenyl	Phenyl	3.7594(9)	0.00(7)	22.4	22.4	1.430	1/2 – *x*, 1/2 – *y*, −*z*
*Complex **3***							
Pyrazine	Phenyl	4.062(4)	21.4(3)	20.5	40.1		1 – *x*, 1 – *y*, −*z*
Phenyl	Pyrazine	4.062(4)	21.4(3)	40.1	20.5		1 – *x*, 1 – *y*, −*z*
*Complex **4**·H$_2$O*							
Pyrazine	Phenyl	3.6872(9)	2.27(7)	28.8	26.9	1.774	1 – *x*, 2 – *y*, −*z*
Phenyl	Pyrazine	3.6871(9)	2.27(7)	26.9	28.8	1.667	1 – *x*, 2 – *y*, −*z*
Pyrazine	Phenyl	3.5657(9)	2.27(7)	24.5	23.9	1.476	2 – *x*, 2 – *y*, −*z*
Phenyl	Pyrazine	3.5658(9)	2.27(7)	23.9	24.4	1.442	2 – *x*, 2 – *y*, −*z*

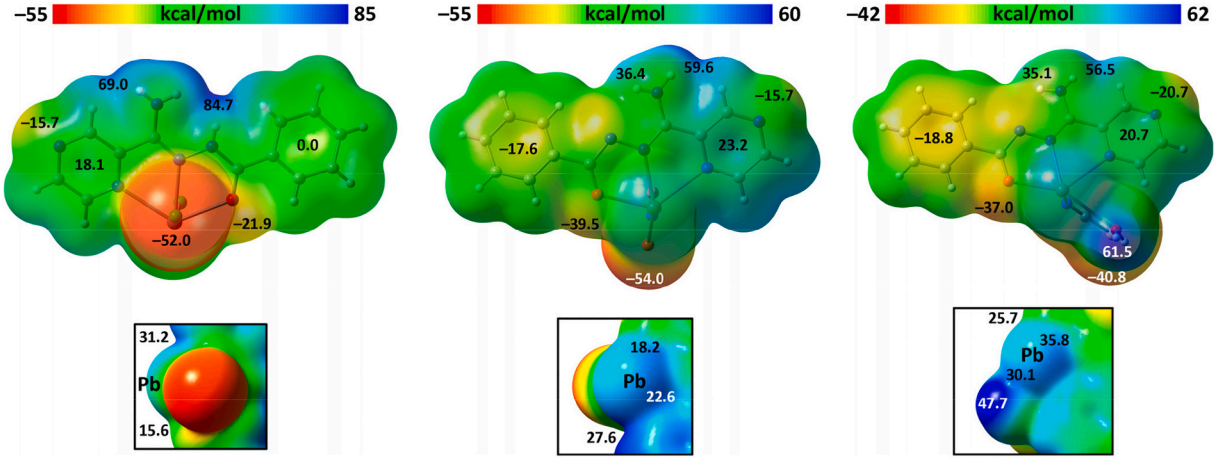

Fig. 6. The MEP surfaces of complexes **1** (left), **3** (middle) and **4** (right). The MEP values at selected points of the surfaces are indicated in kcal/mol. In the lower panels, amplification of the MEP surfaces around the Pb-atoms are shown. In these amplifications, narrow MEP scales were used: ±32 kcal/mol (left) ±27 kcal/mol (middle) and ± 40 kcal/mol (right).

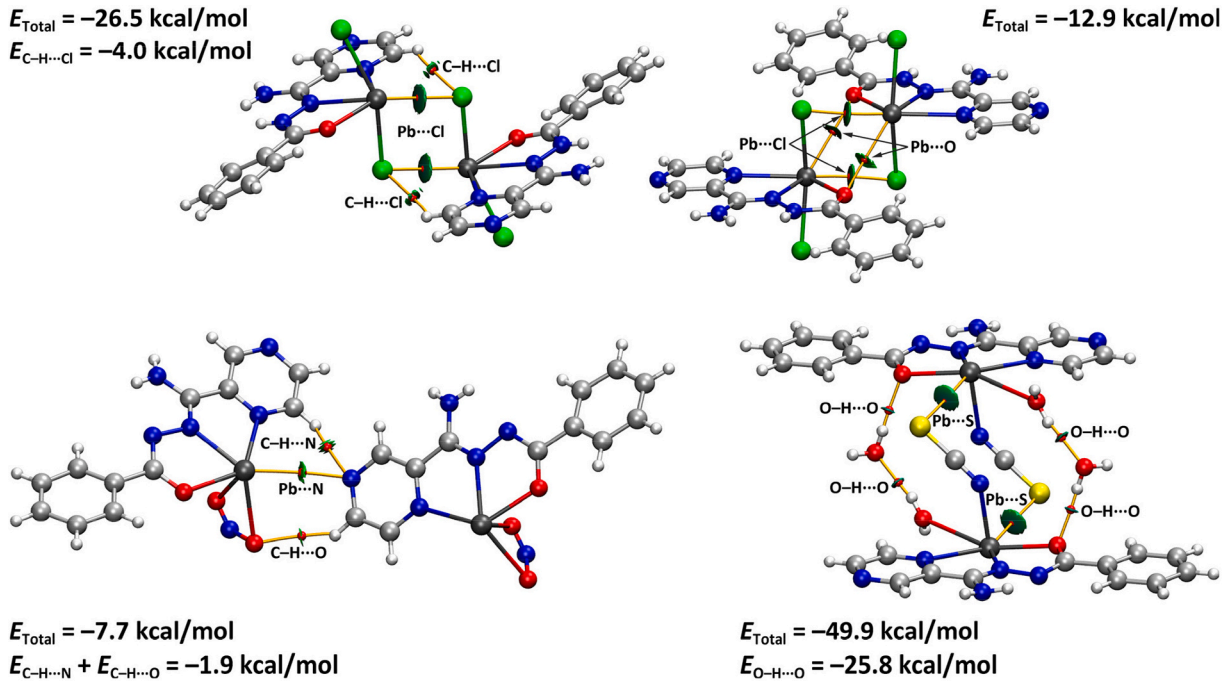

Fig. 7. The QTAIM/NCIplot analysis of two self-assembled tetrel-bonded dimers of complexes **1** (top), **3** (bottom-left) and **4** (bottom-right). Bond critical points and bond paths are shown as small red spheres and orange lines, respectively. (For interpretation of the references to colour in this figure legend, the reader is referred to the web version of this article.)

neighboring molecule (Fig. 7). This central tetrel bond is flanked by two hydrogen bonds, yielding the total dimerization energy for this arrangement of −7.7 kcal/mol (Fig. 7). This value is significantly smaller compared to the dimers of complex **1**, which is attributed to two factors: the presence of only a single tetrel bond in the dimer of **3**, and the lower nucleophilicity of the pyrazine nitrogen atom compared to the chlorine atoms in **1** (Fig. 7). The energetic contribution of the two flanking hydrogen bonds was calculated to be −1.9 kcal/mol, confirming that the Pb···N tetrel bond is the dominant interaction stabilizing this dimer.

The self-assembled dimer of complex **4** is further facilitated by two crystal water molecules (Fig. 7). As anticipated by the blue colour of the reduced density gradient isosurfaces from the NCIPlot, the water molecules form strong hydrogen bonds, which play a crucial role in the dimer's formation. The assembly is stabilized by a combination of two Pb···S tetrel bonds and four strong O–H···O hydrogen bonds (Fig. 7). The total formation energy of this dimer is very large, measuring −49.9 kcal/mol. The contribution of the hydrogen bonds was estimated to be −25.8 kcal/mol by recomputing the assembly without the water molecules and taking the difference. This indicates that in this specific supramolecular arrangement, the hydrogen bonds are slightly stronger than the tetrel bonds, highlighting their significant role in stabilizing the extended structure.

To further analyze the nature of the tetrel bonds, combined 2D plots of the Laplacian of density ($\nabla^2\rho$) and 2D RDG maps were utilized for two model systems of **1** and **4**. This approach helps to distinguish between covalent and noncovalent interactions. Additionally, the 2D ELF map was used to highlight the nucleophilic and electrophilic regions within the dimer. The 2D $\nabla^2\rho$ maps for both complexes **1** and **4** show positive values between the Pb and Cl/S atoms (Fig. 8). This is consistent with

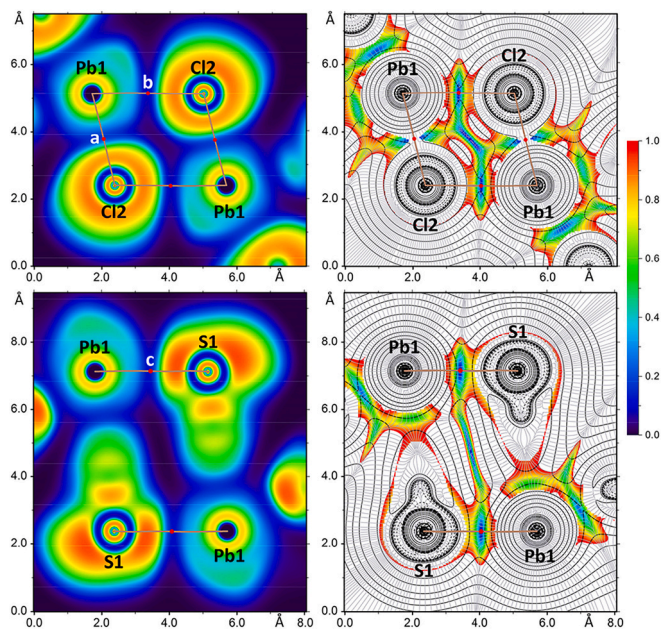

Fig. 8. The ELF (left) and Laplacian/RDG (left) maps for the $[Pb1\cdots Cl2]_2$ dimer of complex **1** (top) and for the $[Pb1\cdots S1]_2$ dimer of complex **4**. Bond critical points and bond paths are shown as small red spheres and brown lines, respectively. The red-orange region in the ELF maps indicates electron localization, while the Laplacian maps show regions of electron concentration (solid line contours) and depletion (dashed line contours). (For interpretation of the references to colour in this figure legend, the reader is referred to the web version of this article.)

both coordination (Pb–Cl2) and tetrel bonds ($Pb\cdots Cl2^{\#2}$) in **1**, and for the $Pb1\cdots S1^{\#7}$ tetrel bonds in **4**. However, the 2D RDG maps provide a clear distinction: only the elongated Pb···Cl tetrel bond in **1** and the Pb···S tetrel bond in **4** show blue isocontours (Fig. 8), which are characteristic of non-covalent interactions. The bond critical points and bond paths align with the zero-flux boundaries between the Pb and Cl/S atoms, where RDG values approach zero. The 2D ELF map further clarifies the nature of the bonds. It shows high electron localization at the negative belt of the chlorine atom and the lone pairs of the sulfur atom, while the Pb atom shows an electrophilic character. The ELF values indicate that the coordination bonds, particularly the Pb1–N12 and Pb-Cl2 bonds, are higher than those of the tetrel bonds (Table 4), reflecting greater electron localization and sharing in the coordination bonds.

The QTAIM and ELF parameters (Table 4) confirm the classification of the Pb1–N12 and Pb1–Cl2 bonds as pure coordination bonds and the $Pb1\cdots Cl2^{\#2}$ and $Pb1\cdots S1^{\#7}$ interactions as non-covalent tetrel bonds. This is supported by several key parameters for the tetrel bonds, including an electron density (ρ(r)) value of less than 0.020 a.u. and small positive $\nabla^2\rho$ values (Table 4). For these tetrel bonds, the absolute value of the potential energy density (|V(r)|) is approximately equal to the kinetic energy density (G(r)) at the bond critical points, which is a hallmark of non-covalent interactions (Table 4). A comparative analysis of the obtained data reveals significant differences between the coordination and tetrel bonds (Table 4). The coordination bonds exhibit markedly higher values for ρ(r), $\nabla^2\rho$, V(r), G(r) and the second eigenvalue of the Hessian matrix (λ_2). The total energy density (H(r)) is negative for the coordination bonds, indicating a greater degree of covalency. Finally, the negative λ_2 values across all bonds confirm the presence of attractive forces, with larger values for the coordination bonds reflecting their much stronger nature.

4. Conclusions

In this work, new lead(II) coordination compounds, $[Pb(HL)Cl_2]$ (**1**), $[Pb(HL)_2(NO_3)_2]$ (**2**), $[PbL(NO_2)]$ (**3**) and $[PbL(NCS)(H_2O)]\cdot H_2O$ (**4**·H_2O), were synthesized by reacting aqueous solutions of PbX_2 (X = Cl^-, NO_3^-, SCN^-) or a $Pb(NO_3)_2$ and $NaNO_2$ mixture with a methanolic solution of *N*′-benzoylpyrazine-2-carbohydrazonamide (**HL**). The resulting orange or yellow crystals were suitable for single-crystal X-ray diffraction without recrystallization.

Elemental analysis, FTIR and ^{1}H NMR spectroscopy confirmed the complexes' formation and structures. Complexes **1** and **2** contain the neutral ligand **HL**, while complexes **3** and **4**·H_2O contain the deprotonated form **L**, suggesting Pb^{2+}–NO_2^- and Pb^{2+}–NCS^- systems induce **HL** deprotonation. FTIR spectra confirmed this: complexes **1** and **2** showed a carbonyl band around 1670–1675 cm^{-1}, which is shifted to higher wavenumbers, while complexes **3** and **4**·H_2O showed it around 1620 cm^{-1}, which is shifted to lower wavenumbers in comparison to that in the free parent ligand **HL**. The ^{1}H NMR spectra supported the ligand forms in the reported complexes. Particularly, the spectra of complexes **1** and **2** showed signals for the amide NH hydrogen, while the same signal was absent in the spectra of complexes **3** and **4**·H_2O.

In all complexes, the Pb^{2+} cation is *N*,*N*′,*O*-chelated by the corresponding organic ligand's pyrazine and imine nitrogen, and carbonyl oxygen atoms. Bond length analysis revealed that the Pb–$N_{pyrazine}$, Pb–N_{imine} and Pb–$O_{carbonyl}$ bonds are the longest in complex **2**, which contains two neutral **HL** ligands. Complex **1** shows intermediate lengths, while complexes **3** and **4**·H_2O, both containing deprotonated ligand **L**, have shorter Pb–N_{imine} and Pb–$O_{carbonyl}$ bonds. A significant difference of ~0.35 Å exist in the Pb-Cl bond lengths in complex **1**.

Complex **3** features a disordered nitrite oxygen and chelating nitrito coordination. The nitrate anions in complex **2** are coordinated anisobidentately. Complex **4**·H_2O shows a monodentate N-bound isothiocyanate anion and a long Pb-O water bond of ~2.90 Å. Large gaps in the coordination spheres of complexes **1**, **3** and **4**·H_2O enable the formation of Pb···X tetrel bonds (X = Cl, N, O, S) with adjacent molecules. Combining covalent and tetrel bonds, the coordination environments are described as N_2OCl_4 for **1**, N_4O_6 for **2**, N_4O_4 for **3** and N_5O_2S for **4**·H_2O. These tetrel bonds create 1D supramolecular chains in the structures of complexes **1** and **4**·H_2O or a 2D sheet in the structure of complex **3**. All complexes form extended structures through hydrogen bonds involving NH_2 and NH groups and a variety of acceptor atoms. Pyrazine–phenyl π···π interactions further stabilize all structures, supplemented by phenyl–phenyl interactions in complexes **1** and **2**.

The MEP surface analysis showed that the Pb atom has an anisotropic charge distribution, with distinct regions of positive potential (σ-holes) that are well-suited for forming tetrel bonds. This analysis also identified key hydrogen bond donor and acceptor sites, and aromatic rings capable of π···π interactions. Dimerization energy calculations and QTAIM/NCIplot analyses confirmed the presence of strong attractive Pb···X

Table 4
QTAIM and ELF values (a.u.) for the specified bond critical points (BCPs) in complexes **1** and **4**.

Complex	BCP	ρ(r)	G(r)	V(r)	H(r)	$\nabla^2\rho$	ELF	λ_2
1	Pb1–N12	0.0463	0.0387	−0.0433	−0.0046	0.1360	0.1644	−0.0493
	Pb1···Cl2	0.0410	0.0280	−0.0320	−0.0049	0.0926	0.2002	−0.0344
4	$Pb1\cdots Cl2^{\#2}$	0.0163	0.0095	−0.0087	0.0008	0.0414	0.0894	−0.0109
	$Pb1\cdots S1^{\#7}$	0.0164	0.0080	−0.0078	0.0002	0.0328	0.1257	−0.0115

tetrel bonds (X = Cl, N, S) as a primary driving force for supramolecular assembly. For the dimers of complexes **1** and **3**, the tetrel bonds were found to be the dominant interactions, despite the presence of ancillary hydrogen bonds. In the tetramer of complex **4**, however, the strong O-H···O hydrogen bonds contributed a significant portion of the total stabilization energy, making them slightly stronger than the tetrel bonds. Finally, the 2D ELF and Laplacian maps distinguished the non-covalent character of the tetrel bonds from the more covalent nature of the primary Pb-N and Pb-O coordination bonds, supported by quantitative QTAIM data showing much higher electron density and covalency for the coordination bonds. These theoretical findings complement the experimental data by providing a comprehensive understanding of the complex interplay of forces that dictate the crystal packing in these materials.

Ultimately, we believe that this research provides valuable insights for the ongoing quest in coordination chemistry and crystal engineering to identify and strategically employ both primary and auxiliary ligands. The detailed structural and supramolecular findings presented here, encompassing diverse coordination environments, ligand deprotonation effects, anion interactions and the deliberate formation of tetrel bonds, offer concrete design principles and empirical data. These will directly aid researchers in the rational design and successful construction of novel coordination polymers and extended architectures with targeted properties.

CRediT authorship contribution statement

Ghodrat Mahmoudi: Investigation, Formal analysis, Conceptualization. **Isabel Garcia-Santos:** Supervision, Investigation, Funding acquisition, Conceptualization. **Alfonso Castiñeiras:** Visualization, Investigation, Funding acquisition, Conceptualization. **Atash V. Gurbanov:** Validation, Methodology, Investigation, Formal analysis. **Ömer Faruk Tutar:** Visualization, Methodology, Investigation, Formal analysis. **Elizaveta V. Panova:** Visualization, Investigation, Formal analysis, Data curation, Conceptualization. **Rosa M. Gomila:** Visualization, Validation, Software, Investigation, Formal analysis, Conceptualization. **Antonio Frontera:** Writing – review & editing, Supervision, Investigation, Funding acquisition. **Damir A. Safin:** Writing – review & editing, Writing – original draft, Visualization, Validation, Supervision, Investigation, Funding acquisition, Formal analysis.

Declaration of competing interest

The authors declare that they have no known competing financial interests or personal relationships that could have appeared to influence the work reported in this paper.

Acknowledgements

This work was supported by the grant from the Russian Science Foundation (No. 24-23-00118). I. Garcia-Santos thanks Conselleria de Cultura, Educacion, Formacion Profesional e Universidades, Xunta de Galicia (ED431B 2023/19). Atash V. Gurbanov is grateful to the Baku State University. This research was funded by the MICIU/AEI of Spain (project PID2023-148453NB-I00, FEDER funds)

Appendix A. Supplementary data

Supplementary data to this article can be found online at https://doi.org/10.1016/j.inoche.2025.116058.

Data availability

All the data is available in the manuscript or attached X-ray files

References

[1] Y.H. Zhao, H.B. Xu, Y.M. Fu, K.Z. Shao, S.Y. Yang, Z.M. Su, X.R. Hao, D.X. Zhu, E. B. Wang, A series of lead(II)-organic frameworks based on pyridyl carboxylate acid N-oxide derivatives: syntheses, structures, and luminescent properties, Cryst. Growth Des. 8 (2008) 3566–3576.
[2] V. Stavila, K.H. Whitmire, I. Rusakova, Synthesis of Bi_2S_3 nanostructures from bismuth(III) thiourea and thiosemicarbazide complexes, Chem. Mater. 21 (2009) 5456–5465.
[3] X.L. Wang, Y.Q. Chen, Q. Gao, H.Y. Lin, G.C. Liu, J.X. Zhang, A.X. Tian, Coordination behavior of 5,6-substituted 1,10-phenanthroline derivatives and structural diversities by coligands in the construction of lead(II) complexes, Cryst. Growth Des. 10 (2010) 2174–2184.
[4] C.P. Li, Q. Yu, J. Chen, M. Du, Supramolecular coordination complexes with 5-sulfoisophthalic acid and 2,5-bipyridyl-1,3,4-oxadiazole: specific sensitivity to acidity for Cd(II) species, Cryst. Growth Des. 10 (2010) 2650–2660.
[5] A.C. Wibowo, S.A. Vaughn, M.D. Smith, H.-C. Zur Loye, Novel bismuth and Lead coordination polymers synthesized with pyridine-2,5-dicarboxylates: two single component "white" light emitting phosphors, Inorg. Chem. 49 (2010) 11001–11008.
[6] J. He, M. Zeller, A.D. Hunter, Z. Xu, White light emission and second harmonic generation from secondary group participation (SGP) in a coordination network, J. Am. Chem. Soc. 134 (2012) 1553–1559.
[7] Y.X. Tan, F.Y. Meng, M.C. Wu, M.H. Zeng, Two Pb(II) dicarboxylates constructed by rigid terephthalate or flexible D(+)-camphorate with different 3D motif based on cooperative effect of steric hindrance of ligand and lone pair electrons, J. Mol. Struct. 928 (2009) 176–181.
[8] A. Bauzá, T.J. Mooibroek, A. Frontera, Tetrel bonding interactions, Chem. Rec. 16 (2016) 473–487.
[9] G. Mahmoudi, A. Bauza, M. Amini, E. Molins, J.T. Mague, A. Frontera, On the importance of tetrel bonding interactions in lead(II) complexes with (iso) nicotinohydrazide based ligands and several anions, Dalton Trans. 45 (2016) 10708–10716.
[10] G. Mahmoudi, A.V. Gurbanov, S.R. Hemida, R. Corballo, M. Amini, A. Bacchi, M. P. Mitoraj, F. Sagan, M. Kukulka, D.A. Safin, Ligand-driven coordination sphere-induced engineering of hHybride materials constructed from $PbCl_2$ and bis-pyridyl organic linkers for single-component light-emitting phosphors, Inorg. Chem. 56 (2017) 9698–9709.
[11] G. Mahmoudi, D.A. Safin, M.P. Mitoraj, M. Amini, M. Kubicki, T. Doert, F. Locherere, M. Fleck, Anion-driven tetrel bond-induced engineering of lead(II) architectures with N′-(1-(2-pyridyl)ethylidene)nicotinohydrazide: experimental and theoretical findings, Inorg. Chem. Front. 4 (2017) 171–182.
[12] G. Mahmoudi, E. Zangrando, M.P. Mitoraj, A.V. Gurbanov, F.I. Zubkov, M. Moosavifar, I.A. Konyaeva, A.M. Kirillov, D.A. Safin, Extended lead(II) architectures engineered via tetrel bonding interactions, New J. Chem. 42 (2018) 4959–4971.
[13] M. Servati Gargari, V. Stilinović, A. Bauzá, A. Frontera, P. McArdle, D. Van Derveer, S.W. Ng, G. Mahmoudi, Design of lead(II) metal–organic frameworks based on covalent and tetrel bonding, Chem. Eur. J. 21 (2015) 17951–17958.
[14] S. Roy, M.G.B. Drew, A. Bauzá, A. Frontera, S. Chattopadhyay, Non-covalent tetrel bonding interactions in hemidirectional lead(II) complexes with nickel(II)-salen type metalloligands, New J. Chem. 42 (2018) 6062–6076.
[15] A. Franconetti, A. Frontera, "Like–like" tetrel bonding interactions between Sn centres: a combined ab initio and CSD study, Dalton Trans. 48 (2019) 11208–11216.
[16] A. Bauzá, S.K. Seth, A. Frontera, Tetrel bonding interactions at work: impact on tin and lead coordination compounds, Coord. Chem. Rev. 384 (2019) 107–125.
[17] J.F. Keggin, F.D. Miles, Structures and formulæ of the prussian blues and related compounds, Nature 137 (1936) 577–578.
[18] Y. Kinoshita, I. Matsubara, T. Higuchi, Y. Saito, The crystal structure of bis (adiponitrilo)copper(I) nitrate, Bull. Chem. Soc. Jpn. 32 (1959) 1221–1226.
[19] O.M. Yaghi, H. Li, Hydrothermal synthesis of a metal-organic framework containing large rectangular channels, J. Am. Chem. Soc. 117 (1995) 10401–10402.
[20] O.M. Yaghi, G. Li, H. Li, Selective binding and removal of guests in a microporous metal-organic framework, Nature 378 (1995) 703–706.
[21] S.R. Batten, N.R. Champness, X.-M. Chen, J. Garcia-Martinez, S. Kitagawa, L. Öhrström, M. O'Keeffe, M.P. Suh, J. Reedijk, Terminology of metal–organic frameworks and coordination polymers (IUPAC Recommendations 2013), Pure Appl. Chem. 85 (2013) 1715–1724.
[22] J. Zhao, J. Yuan, Z. Fang, S. Huang, Z. Chen, F. Qiu, C. Lu, J. Zhu, X. Zhuang, One-dimensional coordination polymers based on metal–nitrogen linkages, Coord. Chem. Rev. 471 (2022) 214735.
[23] N. Dunski, T.H. Crawford, Coordination polymers of Schiff base ligands and their monomeric analogs, J. Inorg. Nucl. Chem. 35 (1973) 2707–2717.
[24] G. Mahmoudi, A.A. Khandar, J. White, M.P. Mitoraj, H.S. Jena, P. Van Der Voort, N. Qureshi, A.M. Kirillov, K. Robeyns, D.A. Safin, Polar protic solvent-trapping polymorphism of the Hg^{II}-hydrazone coordination polymer: experimental and theoretical findings, CrystEngComm 19 (2017) 3017–3025.
[25] J.D. Velásquez, G. Mahmoudi, E. Zangrando, A.V. Gurbanov, F.I. Zubkov, Y. Zorlu, A. Masoudiasl, J. Echeverría, Experimental and theoretical study of Pb···S and Pb···O σ-hole interactions in the crystal structures of Pb(II) complexes, CrystEngComm 21 (2019) 6018–6025.
[26] G. Mahmoudi, F.A. Afkhami, A. Kennedy, F.I. Zubkov, E. Zangrando, A.M. Kirillov, E. Molins, M.P. Mitoraj, D.A. Safin, Lead(II) coordination polymers driven by

pyridine-hydrazine donors: from anion-guided self-assembly to structural features, Dalton Trans. 49 (2020) 11238–11248.
[27] G. Mahmoudi, A. Masoudiasl, M.G. Babashkina, A. Frontera, T. Doert, J.M. White, E. Zangrando, F.I. Zubkov, D.A. Safin, On the importance of π-hole spodium bonding in tricoordinated Hg^{II} complexes, Dalton Trans. 49 (2020) 17547–17551.
[28] F.A. Afkhami, G. Mahmoudi, F. Qu, A. Gupta, M. Köse, E. Zangrando, F.I. Zubkov, I. Alkorta, D.A. Safin, Supramolecular lead(II) architectures engineered by tetrel bonds, CrystEngComm 22 (2020) 2389–2396.
[29] G. Mahmoudi, M. Abedi, S.E. Lawrence, E. Zangrando, M.G. Babashkina, A. Klein, A. Frontera, D.A. Safin, Tetrel bonding and other non-covalent interactions assisted supramolecular aggregation in a new Pb(II) complex of an isonicotinohydrazide, Molecules 25 (2020) 4056.
[30] G. Mahmoudi, F.A. Afkhami, E. Zangrando, W. Kaminsky, A. Frontera, D.A. Safin, A supramolecular 3D structure constructed from a new metal chelate self-assembled from $Sn(NCS)_2$ and phenyl(pyridin-2-yl)methylenepicolinohydrazide, J. Mol. Struct. 49 (2020) 129188.
[31] G. Mahmoudi, M. Kubicki, D. Choquesillo-Lazarte, B. Miroslaw, E.V. Alexandrov, P. N. Zolotarev, A. Frontera, D.A. Safin, Supramolecular architectures of $Mn(NCS)_2$ complexes with N′-(1-(pyridin-4-yl)ethylidene)picolinohydrazide and N′-(phenyl (pyridin-4-yl)methylene)isonicotinohydrazide, Polyhedron 190 (2020) 114776.
[32] F.A. Afkhami, G. Mahmoudi, F. Qu, A. Gupta, E. Zangrando, A. Frontera, D. A. Safin, Supramolecular architecture constructed from the hemidirected lead(II) complex with N′-(4-hydroxybenzylidene)isonicotinohydrazide, Inorg. Chim. Acta 502 (2020) 119350.
[33] J.D. Velásquez, G. Mahmoudi, E. Zangrando, B. Miroslaw, D.A. Safin, J. Echeverría, Non-covalent interactions induced supramolecular architecture of $Hg(NCS)_2$ with 3-pyridinecarbaldehyde nicotinoylhydrazone, Inorg. Chim. Acta 509 (2020) 119700.
[34] G. Mahmoudi, A. Masoudiasl, F.A. Afkhami, J.M. White, E. Zangrando, A. V. Gurbanov, A. Frontera, D.A. Safin, A new coordination polymer constructed from $Pb(NO_3)_2$ and a benzylideneisonicotinohydrazide derivative: coordination-induced generation of a π-hole towards a tetrel-bonding stabilized structure, J. Mol. Struct. 1234 (2021) 130139.
[35] V. Alizadeh, G. Mahmoudi, M.A. Vinokurova, K.M. Pokazeev, K.A. Alekseeva, B. Miroslaw, A.A. Khandar, A. Frontera, D.A. Safin, Spodium bonds and metal–halogen···halogen–metal interactions in propagation of monomeric units to dimeric or polymeric architectures, J. Mol. Struct. 1252 (2022) 132144.
[36] I. Garcia-Santos, A. Castiñeiras, G. Mahmoudi, M.G. Babashkina, E. Zangrando, R. M. Gomila, A. Frontera, D.A. Safin, Supramolecular aggregation of lead(II) perchlorate and a thiosemicarbazide derivative linked by a myriad of non-covalent interactions, Inorg. Chim. Acta 538 (2022) 120974.
[37] G. Mahmoudi, I. Garcia-Santos, M. Pittelkow, F.S. Kamounah, E. Zangrando, M. G. Babashkina, A. Frontera, D.A. Safin, The tetrel bonding role in supramolecular aggregation of lead(II) acetate and a thiosemicarbazide derivative, Acta Cryst. B78 (2022) 685–694.
[38] I. Garcia-Santos, A. Castiñeiras, G. Mahmoudi, M.G. Babashkina, E. Zangrando, R. M. Gomila, A. Frontera, D.A. Safin, An extended supramolecular coordination compound produced from $PbCl_2$ and N′-isonicotinoylpicolinohydrazonamide, CrystEngComm 24 (2022) 368–378.
[39] G. Mahmoudi, E. Zangrando, A.V. Gurbanov, B. Eftekhari-Sis, M.P. Mitoraj, F. Sagan, D.A. Safin, Tetrel bonding stabilization of a new coordination polymer constructed from lead(II) azide and 1-(pyridin-2-yl)ethylidenepicolinohydrazide, CrystEngComm 25 (2023) 5100–5108.
[40] I. Garcia-Santos, T. Iglesias-Pereiro, E. Labisbal, A. Castiñeiras, B. Eftekhari-Sis, G. Mahmoudi, F. Sagan, M.P. Mitoraj, D.A. Safin, An extended supramolecular coordination compound produced from $PbCl_2$ and N′-isonicotinoylpicolinohydrazonamide, CrystEngComm 26 (2024) 1252–1260.
[41] B. Eftekhari-Sis, I. Garcia-Santos, A. Castiñeiras, G. Mahmoudi, E. Zangrando, A. Frontera, D.A. Safin, On the pivotal role of tetrel bonding in the supramolecular architectures of Pb^{II}–NCS complexes with chelating thiosemicarbazide derivatives, CrystEngComm 26 (2024) 1637–1646.
[42] G. Mahmoudi, I. Garcia-Santos, E. Labisbal, A. Castiñeiras, V. Alizadeh, R. M. Gomila, A. Frontera, D.A. Safin, A lead(II)–N′-isonicotinoylpyrazine-2-carbohydrazonamide complex system as a converter of aerial carbon dioxide to carbonate under electrochemical conditions with the formation of a single-component white light-emitting phosphor, CrystEngComm 26 (2024) 4205–4213.
[43] G. Mahmoudi, I. Garcia-Santos, A. Castiñeiras, R. Fernández-Vazquez, M. S. Gargari, R.M. Gomila, A. Frontera, D.A. Safin, Anion driven tetrel bonding dictated supramolecular architectures of lead(II) with a zwitterionic form of polydentate N′-(piperidine-1-carbonothioyl)picolinohydrazonamide, CrystEngComm 26 (2024) 4357–4366.
[44] G. Mahmoudi, I. Garcia-Santos, E. Labisbal, A. Castiñeiras, V. Alizadeh, R. M. Gomila, A. Frontera, D.A. Safin, Aerial carbon dioxide conversion to carbonate mediated by a lead(II) complex with tridentate bipyridine containing a hydrazide ligand under electrochemical conditions yielding single-component white-light-emitting phosphors, Inorg. Chem. Front. 11 (2024) 6135–6145.
[45] G. Mahmoudi, I. Garcia-Santos, E. Labisbal, A. Castiñeiras, V. Alizadeh, R. M. Gomila, A. Frontera, D.A. Safin, A nanosized porous supramolecular lead(II)–*N′*-phenyl(pyridin-2-yl)methylene-*N*-phenylthiosemicarbazide aggregate, obtained under electrochemical conditions, Inorg. Chem. 63 (2024) 18581–18588.
[46] G. Mahmoudi, I. Garcia-Santos, D.A. Safin, R. Fernández-Vazquez, B. Eftekhari-sis, R.M. Gomila, A. Frontera, A joint action of coordination, hydrogen and tetrel bonds toward a new 2D coordination polymer of lead(II) perchlorate and *N′*-isonicotinoylpyrazine-2-carbohydrazonamide, Inorg. Chem. Commun. 174 (2025) 113914.
[47] G. Mahmoudi, I. Garcia-Santos, T. Iglesias-Pereiro, A. Castiñeiras, J. Corredoira-Vázquez, A.V. Gurbanov, E. Zangrando, R.M. Gomila, A. Frontera, D.A. Safin, A supramolecular coordination polymer incorporating lead(II) perchlorate, amino (pyridin-2-yl)methylenepyridin-1-ium-4-carbohydrazonate and thiocyanate as an auxiliary ligand, Inorg. Chem. Commun. 180 (2025) 114905.
[48] E.V. Panova, T.M. Burkhanova, D.A. Safin, A mononuclear homoleptic complex of *N′*-(4-hydroxybenzylidene)isonicotinohydrazide with lead(II): experimental and in silico studies, Russ. J. Phys. Chem. A 99 (2025) 786–794.
[49] G. Mahmoudi, I. Garcia-Santos, T. Iglesias-Pereiro, A. Castiñeiras, J. Corredoira-Vázquez, A.V. Gurbanov, E. Zangrando, R.M. Gomila, A. Frontera, D.A. Safin, Interaction of Llead(II) perchlorate with *N′*-isonicotinoylpicolinohydrazonamide and its sodium salt in the presence of potassium cyanide: yellow green light emitting phosphors, stabilized by tetrel bonds, and a system to transform methanol to acetate, Inorg. Chem. 64 (2025) 14670–14683.
[50] G. Mahmoudi, I. Garcia-Santos, A. Castiñeiras, M. Servati Gargari, A. Frontera, D. A. Safin, Novel benzoyl and acetyl pyrazine-2-carbohydrazonamide hybrid derivatives: experimental and theoretical insights, Inorg. Chem. Commun. 169 (2024) 112990.
[51] APEX2 Software, Bruker AXS Inc, Madison, Wisconsin, USA, 2017.
[52] G.M. Sheldrick, SADABS, Bruker AXS Inc., Madison, WI-53719, USA, 1997.
[53] G.M. Sheldrick, A short history of SHELXL, Acta Cryst A64 (2008) 112–122.
[54] C. Adamo, V. Barone, Toward reliable density functional methods without adjustable parameters: the PBE0 model, J. Chem. Phys. 110 (1999) 6158–6170.
[55] F. Weigend, Accurate coulomb-fitting basis sets for H to Rn, Phys. Chem. Chem. Phys. 8 (2006) 1057–1065.
[56] E. Caldeweyher, C. Bannwarth, S. Grimme, Extension of the D3 dispersion coefficient model, J. Chem. Phys. 147 (2017) 034112.
[57] R. Ahlrichs, M. Bär, M. Häser, H. Horn, C. Kölmel, Electronic structure calculations on workstation computers: the program system Turbomole, Chem. Phys. Lett. 162 (1989) 165–169.
[58] R.F.W. Bader, A quantum theory of molecular structure and its applications, Chem. Rev. 91 (1991) 893–928.
[59] J. Contreras-García, E.R. Johnson, S. Keinan, R. Chaudret, J.P. Piquemal, S. D. Popelier, W. Yang, NCIPLOT: a program for the visualization of noncovalent interactions, J. Chem. Theory Comput. 7 (2011) 625–632.
[60] A.D. Becke, K.E. Edgecombe, A simple measure of electron localization in atomic and molecular systems, J. Chem. Phys. 92 (1990) 5397–5403.
[61] T. Lu, F. Chen, Multiwfn: a multifunctional wavefunction analyzer, J. Comput. Chem. 33 (2012) 580–592.
[62] W. Humphrey, A. Dalke, K. Schulten, VMD: visual molecular dynamics, J. Mol. Graph. 14 (1996) 33–38.
[63] O. Semyonov, K.A. Lyssenko, D.A. Safin, Copper(II) acetate structures with benzimidazole derivatives, Inorg. Chim. Acta 488 (2019) 238–245.
[64] M. Llunell, D. Casanova, J. Cirera, P. Alemany, S. Alvarez, SHAPE v. 2.1, University of Barcelona, Barcelona, Spain, 2013.
[65] E. Espinosa, E. Molins, C. Lecomte, Hydrogen bond strengths revealed by topological analyses of experimentally observed electron densities, Chem. Phys. Lett. 285 (1998) 170–173.